Journal of Volcanology and Geothermal Research 450 (2024) 108087

Contents lists available at ScienceDirect

Journal of Volcanology and Geothermal Research

journal homepage: www.journals.elsevier.com/journal-of-volcanology-and-geothermal-research

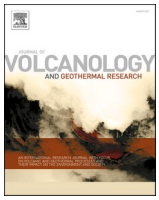

# Brittle fragmentation of Fissure 17 enclave magma revealed by fractal analysis

V. Haag [a,*], B.F. Houghton [b], D. Perugini [c], A. Soldati [a]

[a] Department of Marine, Earth, and Atmospheric Sciences, North Carolina State University, United States of America
[b] Department of Earth Sciences, University of Hawaii, United States of America
[c] Department of Physics and Geology, University of Perugia, Italy

ARTICLE INFO

*Keywords:*
Enclaves
Fractals
Brittle fragmentation
Magma mixing
Kilauea 2018
F17

ABSTRACT

The 2018 LERZ eruption of Kilauea featured a wide range of eruptive styles. In particular, Fissure 17 (F17) displayed activity ranging from Hawaiian fountaining in the eastern part of the fissure to Strombolian explosions in the western part. Lava erupted from F17-West was highly viscous and contained magmatic enclaves. Magmatic enclaves have previously been observed in many other volcanic systems (e.g. Vulcano Island, IT and Sete Cidades Volcano, PT), where they have been attributed to injection of mafic magma into an evolved magma chamber, resulting in viscous fingering, quenching, and break-off into fragments. The F17 enclaves differ from previous studies in that the chemical compositions of the enclave and host magmas are very similar, and that the enclaves have a limited spatial distribution and lack signs of viscous behavior and quenching, pointing to a different formation mechanism than inferred for other volcanic systems.

In order to test a different formation hypothesis, we conducted fractal analysis of the size distribution of 84 individual enclaves from F17-West lavas. Our results, including a fractal dimension of fragmentation $D_f$ of 2.59, indicate that the F17 enclaves likely formed by brittle fragmentation. Since the enclave and host magmas were at temperatures far above the glass transition during the magma hybridization, high strain rates have to be invoked to explain the brittle fragmentation. This may have caused the enclave magma to transition into solid-state behavior, allowing it to break off into fragments that were subsequently picked up by the host magma and carried to the free surface.

The enclaves from F17-West therefore offer a unique insight into the diversity of processes that characterizes the shallow parts of volcanic systems, as well as the importance of strain rates in modulating the rheological behavior of magmas.

## 1. Introduction

### 1.1. The 2018 Kilauea eruption

The 2018 Lower East Rift Zone (LERZ) Kilauea eruption joined ongoing activity at the Halema'uma'u summit crater and the Middle East Rift Zone (MERZ) Pu'u 'O'o cone. On April 30, 2018, the Pu'u 'O'o crater floor collapsed, and geophysical methods indicated an intrusion of magma downrift towards the Lower East Rift Zone (Neal et al., 2018). The first LERZ fissure opened on May 3 at Leilani Estates and was followed by 23 other fissures over the course of the eruption, which ended on September 4. From May to August, lava effusion accompanied collapses at the Halema'uma'u summit (Neal et al., 2018).

Gansecki et al. (2019) divided the eruption into three phases based on the geochemistry of the eruptive products, which indicates magma mixing. Phase 1 lasted from May 3 to May 9 and was marked by the emission of low-temperature silica-rich tholeiite to basaltic andesite lava. At the end of phase 1, the eruptive activity changed to include hotter and less evolved lavas, albeit still more evolved than recent lava found at Pu'u 'O'o and Halema'uma'u. Phase 2 (May 17 to May 27) produced mafic mixed lava in combination with higher effusion rates and reactivation of some uprift vents. Finally, phase 3 (May 28 to August 4) erupted large volumes (92–96% of the total erupted volume) of hot mafic lavas. In addition to these phases, highly evolved lavas (andesites) were erupted from parts of Fissure 17 between May 13 and May 25. Gansecki et al. (2019) found that a mixing continuum between phase 1

* Corresponding author.
*E-mail address:* vehaag@ncsu.edu (V. Haag).

https://doi.org/10.1016/j.jvolgeores.2024.108087
Received 19 January 2024; Received in revised form 29 March 2024; Accepted 25 April 2024
Available online 26 April 2024

and phase 3 magmas could explain the compositions identified at late phase 1 and phase 2, but that these magmas also seemed to have mixed with the andesite at Fissure 17. They propose that the eruption was fed by three different magma sources (Gansecki et al., 2019). Pietruszka et al. (2021) found that the hot mafic lava associated with phase 2 and 3 was likely the result of mixing between three components, including magma derived from the summit, an older and more differentiated magma previously stored in the ERZ, and olivine, creating a large magmatic body in the Middle East Rift Zone (MERZ).

According to Neal et al. (2018), the LERZ eruption was impacted by a feedback process driven by these summit collapses. While the ERZ was most likely primed for an eruption before the onset of the 2018 event, the summit collapse might have impacted magma migration and caused pulses in lava effusion at the ERZ. This has been independently inferred by Patrick et al. (2019) as well, who found that the activity at Fissure 8 (where most of the magma was erupted) fluctuated in both a short-term ("pulses") and a long-term ("surges") manner. The authors argue that the pulses, with periods of 5–10 min, were the result of variations in outgassing efficiency, while the surges, with periods of 1–2 days, tracked with pressure waves caused by the summit collapses. The summit collapses were not, however, the main driving force of the eruption, forcing summit magma to the LERZ. Rather, Pietruszka et al. (2021) argues that the large magma body in the MERZ was the main source of the erupted magma.

### 1.2. Fissure 17

Fissure 17 (hereafter referred to as F17) was active between May 13 and 25 and was offset ~200 m in a NW direction from the other fissures (Supplementary Fig. 1). Lava emitted at this fissure was more evolved compared to any other 2018 LERZ eruptive products, with chemical compositions ranging from basaltic andesite to andesite (Gansecki et al., 2019). Additionally, F17 displayed a wide variety of eruptive styles ranging from Hawaiian in the eastern part to Strombolian in the western part (Soldati et al., 2021). According to Houghton (pers. comm.), the activity at F17 could be divided into three phases. Phase 1 (May 13 to May 14) displayed heterogeneous activity across the approximately 300 m long fissure, with weak unsteady fountaining in the eastern and central part and Strombolian explosions in the western part of the fissure. During Phase 2 (May 15 to May 20) the fissure could be divided into three segments: segment A included the eastern portion of the fissure, characterized by Hawaiian fountaining and the buildup of a small cone; segment B, the central part of the fissure, displayed alternating activity between rapid Strombolian and unsteady Hawaiian from 3 to 5 vents; and segment C, the western segment of the fissure, consisted of multiple vents with widely-spaced pulsating normal Strombolian explosions. Finally, by phase three (May 21 to May 25), the activity in the eastern segment A had significantly decreased, segment B was no longer active, while segment C continued to display Strombolian activity, albeit with lesser intensity, until May 25.

Gansecki et al. (2019) noted that the varying eruptive styles are consistent with the variable, generally high, silica content of the erupted magma along the fissure. Indeed, Soldati et al. (2021) found that F17 erupted lavas with viscosities 1–2 orders of magnitude higher than other fissures, and that the wide range of silica content at F17 was reflected by in the variable viscosities of the products. The western part of the fissure has higher silica contents (59.75–61.53 wt% $SiO_2$), corresponding to higher viscosities (9200–10,700 Pa s at 1064–1056 °C) than the eastern part (53.33–56.35 wt% $SiO_2$ and 366–776 Pa s at 1117–1102 °C). In addition, Walker et al. (2023) proposed that the varying activity types were related to viscosity, variations in mass flux, and the degree of volatile decoupling from the magma.

Gansecki et al. (2019) hypothesized that the evolved chemical composition of F17 was the result of a magma mixing event as the ascending magma intersected an andesite body left over from a previous eruption. This has been further investigated by Soldati (pers. comm.), who concluded that the chemical compositions are consistent with magma hybridization. However, Soldati (pers. comm.) found that there is a 5–10 wt% difference in SiO2 between the interstitial glasses in the eastern and the western part of the fissure, and that there is limited evidence of magma mixing in the eastern part. As such, the mixing was likely limited to the western and central part of the fissure. The difference in chemistry is consistent with cooling of the western magma due to hybridization with a subvolcanic mush left behind after the 1955 eruption. The mixing of the two magmas caused the temperature of the juvenile magma to decrease below the crystallization temperature of magnetite. Mixing further caused water exsolution, resulting in extensive plagioclase crystallization. The crystalline texture of the new hybridized magma inhibited gas movement which, in combination with bubble nucleation and decoupling due to gas exsolution, contributed to the widely-spaced Strombolian activity in the western part of the fissure (Soldati, pers. comm.).

Much like the 2018 eruption, the 1955 eruption consisted of lavas that were compositionally heterogeneous and were more evolved in the beginning than in the later stages of the eruption. While Wright and Fiske (1971) attributed this variation to magma mixing, Ho and Garcia (1988) found that mineral zonation, chemical data and modeling are inconsistent with this hypothesis, and favored crystal fractionation (Ho and Garcia, 1988). According to Ho and Garcia (1988), the early-stage lavas fractionated from the later-stage lavas, and lavas subsequently erupted in 1961 may have fractionated from 1955 residual magma.

Along with the unusually high silica content and explosive activity, the lava emitted from the western part of F17 also hosted enclaves. These enclaves are reported to be 0.01–10 mm in size, holocrystalline and contain small (10 μm) bubbles which are primarily found around phenocrysts. The phenocrysts are 175 μm on average, while the microlites are 10–15 μm, including partially resorbed clinopyroxenes with $X_{Mg} = 0.74–0.86$ and plagioclase crystals, the most calcic of which with $X_{An} = 0.69–0.74$, some of which are found growing radiating over the border of the enclave into the host magma (Soldati, pers. comm.). The enclaves lack viscous textures at both hand sample and microscopic scale as well as signs of quenching. Additionally, according to the MgO geothermometry of Helz and Thornber (1987), the interstitial glasses of the enclaves yield temperatures of 1019–1035 °C (Soldati et al., 2021).

The enclaves have similar interstitial glass composition to the host magma (andesite-dacite), albeit slightly different glass viscosities (68 Pa s at 1555 °C and 4270 Pa s at 1220 °C) compared to the host glass (110 Pa s at 1555 °C and 3740 Pa s at 1267 °C) (Soldati, pers. comm.).

The enclaves are interpreted to have formed during the hybridization of the western magma – as such originating from the 1955 magma body – and stayed separate from the host magma due to the large difference in viscosity between the two magmas, despite their similar chemistries (Soldati, pers. comm.).

### 1.3. Fractals

Fractals are patterns or shapes that are self-similar across multiple scales. As such, a zoomed-in picture of a perfectly self-similar fractal (e.g. the Koch curve, Mandelbrot, 1982) will still show the same pattern, even though it is at a different scale. Snowflakes, tree branches, and coastlines are examples of natural shapes that display fractal geometries, and, as such, their shapes can be described and quantified using fractal analyses (Mandelbrot, 1982). However, not all natural fractals are perfectly self-similar, and as such, fractals can be more comprehensively defined as patterns deviating from the standard Euclidean dimensions. For example, if the dimension for a line is one and for a plane is two, the dimension of a fractal may fall in between these two values. This dimension, the *fractal dimension (D)*, describes the complexity of the fractal pattern. In the case of a two-dimensional fractal, the fractal dimension is higher for a pattern that is more complex (i.e. closer to a plane) and lower for a pattern that is less complex (i.e. closer to a line) (Mandelbrot, 1982).

Fractal analysis has previously been applied to several topics within the geosciences, including e.g. metamorphic rocks, for which Manning (1994) found that the spacing between metamorphic veins were self-similar, aiding the understanding of fluid flow and metamorphic reactions; sedimentary rocks, for which Katz and Thompson (1985) found that the geometries of pore spaces in sandstones were fractal, and that fractal statistics could be used to predict sandstone porosities; and seismicity, where it has been suggested that there is a self-similarity between the number of earthquakes per year and the magnitude of those earthquakes at any given location (Turcotte, 1989).

Fractal analysis can also be applied to size distributions, such as in the case of island sizes and fragmentation (Mandelbrot, 1982) (Supplementary Fig. 2), the latter yielding the *fractal dimension of fragmentation* ($D_f$). In volcanology, fractal analysis has previously been used to study lava flow margins (e.g. Bruno et al., 1992), pyroclast formation (Perugini and Kueppers, 2012) and viscosity ratios during magma mixing (e.g. Perugini and Poli, 2005). Additionally, previous studies have used $D_f$ to constrain the formation of magmatic enclaves (e.g. Perugini et al., 2007; Paredes-Mariño et al., 2017) using the formula

$$N(R > r) = kr^{-D_f} \tag{1}$$

where $N(R > r)$ is the number $N$ of fragments with a size $R$ that is larger than a comparative size $r$, $k$ is a constant, and $D_f$ is the fractal dimension of fragmentation. This analysis can be used for areas by substituting $R$ and $r$ for $A$ and $a$, respectively, giving the following formula (Mandelbrot, 1982)

$$N(A > a) = ka^{-D_f/2} \tag{2}$$

where $A$ is the area of the object and $a$ is the comparative area. By plotting the logarithm of $logN(A > a)$ against the logarithm of $a$, $D_f$ can be found using the following relationship (Perugini et al., 2007)

$$D_f = -2m \tag{3}$$

where $m$ is the slope of the line.

## 2. Methods

Hand sample-sized enclaves from the western part of Fissure 17 were photographed in the field; a tape measure was included for scale (Fig. 1). The margins of 124 enclaves were manually traced and their areas were calculated using JMicroVision (Roduit, n.d., accessed 2022). After the first tracing iteration, 40 enclaves were excluded from the study due to poorly defined margins and low image resolutions. Thus, 84 enclaves remained that were used for fractal analysis. The tracing was repeated five times for each of these enclaves in order to estimate repeatability, hereafter expressed as standard deviation, and to gain a reliable estimation of enclave area. The scale for each image was manually set anew during each iteration based on the photographed tape measure and as such, following the tracing, the measurements of all iterations were normalized to the average scale.

The fractal dimension of fragmentation was calculated using Eq. (2) by plotting the logarithm of the number $N$ of enclaves with areas $A$ larger than a comparative size $a$ against the logarithm of $a$, after which $D_f$ was found using Eq. (3). The comparative sizes were chosen at equal intervals between the highest and lowest average area found in the data set. Finally, the effective diameter $d$ was found using the following equation, following Hodge and Jellinek (2012)

$$d = \sqrt{A} \tag{4}$$

In order to avoid any data over-manipulation, measurements from each and every individual iteration (420 in total), rather than the average of the iterations, were used when calculating the fractal dimension. During the fractal analysis it became evident that enclaves with an area of $<1$ cm$^2$ did not exhibit a fractal size distribution (Fig. 2). As such, these enclaves were excluded from the calculations of fractal dimension. Additionally, large comparative sizes that were represented by only one measurement, thus yielding $logN(A > a) = 0$, were removed to avoid disproportionate impact of potentially outlying values on the result.

In addition to the fractal dimension, an *elongation value* was calculated according to Perugini et al. (2007), by dividing the average shortest axis with the average longest axis of each enclave. This parameter can have a value between 0 and 1, with smaller values corresponding to larger degrees of elongation. This was done in order to evaluate any elongation processes like viscous fingering.

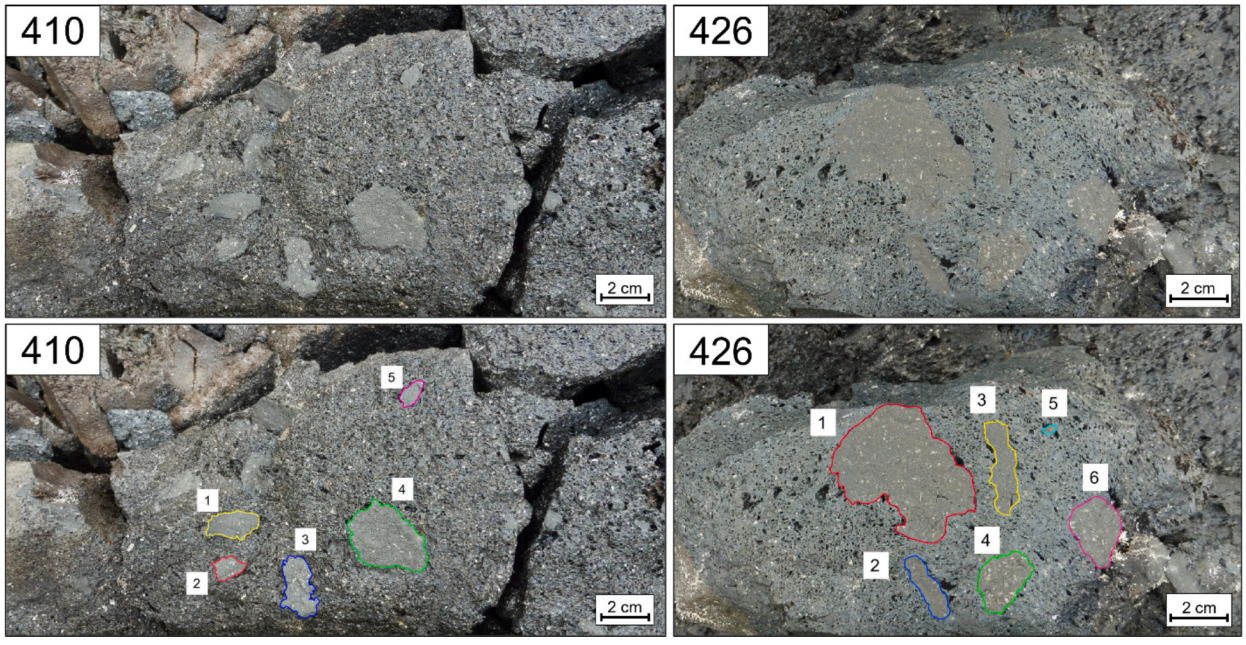


**Fig. 1.** Examples of the enclaves from F17-West (top) and how they were traced (bottom). The numbers in the corners are the names of the images, and the numbers within the image denote the name of each enclave in that image (hereafter indicated as e.g. 410–1).

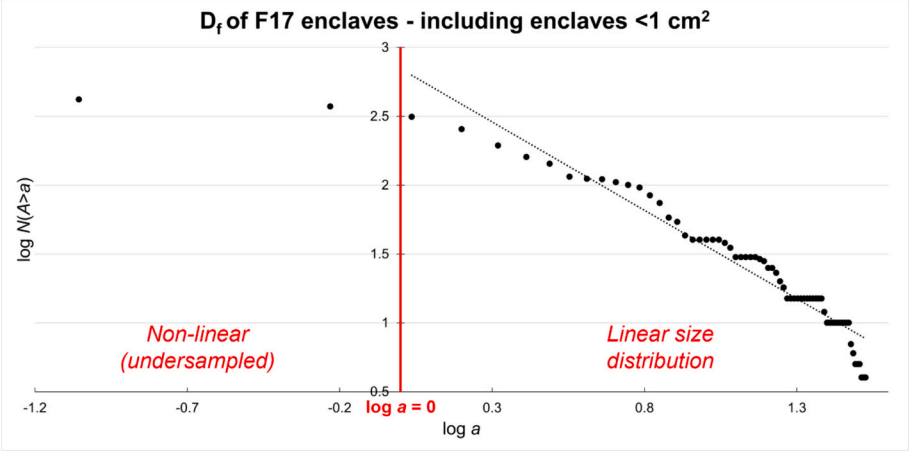


**Fig. 2.** Number of enclaves plotted against each comparative size. Small enclaves deviate from the linear relationship, indicating an incomplete dataset (undersampling). Therefore, enclaves <1cm$^2$ were excluded from the fractal analysis. The linear regression depicted was made solely using data points with log a > 0.

### 2.1. Error assessment

Each enclave was traced five times. The variation between the measurements can be seen in Supplementary Tbl. 1 which includes the average area and standard deviation for each enclave based on the five iterations. On average for all enclaves, the relative standard deviation is 3.675% of the enclave area, and 65 enclaves, corresponding to ~77% of the total, have relative standard deviations of up to 5%. Additionally, to test the impact of excluding the 40 enclaves, the fractal dimension of fragmentation of all 124 enclaves traced in the first iteration were calculated and found to be within the 95% confidence interval (CI) of the fractal dimension of the 84 enclaves (Supplementary Fig. 3). The measurements can thus be considered reliable. However, it is important to acknowledge that, while 84 enclaves is a sizable sample, and the exclusion of the 40 enclaves had little impact, the heterogeneity of the outcrop may mean that our results might not fully capture the complexity of the entire outcrop. Furthermore, we recognize that the size of the enclaves spans just over an order of magnitude. Given the medium through which these enclaves were studied (i.e. photographs) there is an inherent bias towards larger (visible with the naked eye) enclaves, whereas enclaves up to tenths of millimeters in size, such as the microscopic enclaves studied by Soldati (pers. comm.), have been undersampled. It is also important to note that we used a two-dimensional parameter (i.e. area) to characterize three dimensional objects, and that we could not acquire a full view of each enclave. As such, it is impossible in our case to know what section of each enclave we measured (i.e. along the largest axis, shortest axis, or any axis in between). However, this issue is addressed by the assumption that the fractal dimension of a cross section of an object will always be that of the three dimensional shape −1 (thus accommodating for the undersampling of small objects, Glazner and Mills, 2012) and that any object that is fractal will still be fractal no matter how it is viewed (i.e. 2D or 3D; Sreenivasan and Prasad, 1989; Glazner and Mills, 2012). This implies that these uncertainties are not problematic, and that the use of other enclave cross sections would yield similar results.

## 3. Results

The enclaves vary in size between ~0.09 and ~34 cm$^2$. The shapes of the enclaves are mostly determined by the shapes of the crystals which, in some places, are radiating out from the enclave into the host. The enclaves in all iterations have a median area of 1.884 cm$^2$, corresponding to an effective median diameter of 1.373 cm. The frequency histogram plots (Fig. 3, Supplementary Tbl. 2) show that there is a slight bimodality to the size distribution, with a majority of the enclaves with areas between 0 and 10 cm$^2$ clustered between 0 and 4 cm$^2$, and to a lesser degree from 6 and 9 cm$^2$. Considering enclaves with areas between 0 and 30 cm$^2$, they show the lowest frequency between 10 and 14 cm$^2$ and ≥20 cm$^2$. Finally, most enclaves between 0 and 0.99 cm$^2$ are between 0.50 and 0.98 cm$^2$.

The results from the fractal analysis are presented in Fig. 4. The size distribution plots as a linear relationship and the slope of the line ($m = -1.293$) gives $D_f = 2.59$ (95% CI [2.27, 3.28]) for all iterations combined, with an $R^2$ value of 0.938 for the linear relationship. For each iteration separately the fractal dimension is slightly lower, with $D_f = 2.37$ for the first iteration, $D_f = 2.36$ for the second, $D_f = 2.41$ for the third, $D_f = 2.35$ for the fourth, and $D_f = 2.36$ for the fifth. While the size distribution plots as a linear relationship for enclaves ≥1 cm$^2$, when including enclaves <1 cm$^2$ these data points deviate from the linear relationship and plateau (Fig. 2). As such, enclaves <1 cm$^2$ were excluded from all calculations of fractal analysis, corresponding to just under 50% of the analyzed enclaves.

The elongation values range from 0.194 to 0.978 in all iterations, and a chi2 test confirmed that the average values are normally distributed with 95% confidence. The median elongation value of all values in all iterations is 0.596 (Fig. 5).

## 4. Discussion

The fractal dimension of fragmentation has previously been described for multiple materials by Turcotte (1986), who found that the fractal dimension of fragmentation for basalt having undergone brittle fragmentation by means of projectile impacts (Fujiwara et al., 1977) is $D_f = 2.56$, similar to that of granite fragmented in an explosion (Schoutens, 1979) and that of broken coal (Bennet, 1936), both of which have $D_f = 2.50$ (Turcotte, 1986). Additionally, multiple studies have previously applied fractal analysis to constrain the formation mechanism of magmatic enclaves. Perugini and Poli (2000) measured the fractal dimension of element distributions in elemental maps of enclaves. They found that the element distribution is self-similar and proposed that enclaves represent regions that were poorly mixed during magma mixing.

Perugini et al. (2007) used the fractal dimension of fragmentation to compare mafic enclaves in the obsidian Pietre Cotte lava flow (Italy) with enclaves found in the Vegetation Island plutonic outcrops (Antarctica) and found that the areas of the enclaves had $D_f$ of 2.50 and 2.55 respectively, which aligns well with the results found in Turcotte (1986) for brittle fragmentation of basalt. Comparing the $D_f$ of the enclaves at these two sites led to the conclusion that the enclaves in the Pietre Cotte lava flow likely formed during injection of a mafic magma


**Fig. 3.** Frequency histograms of the data in Supplementary Tbl 2. The histograms illustrate the size distribution (area) of the measured enclaves for each iteration (1–5) using different bin ranges. The distribution appears to be somewhat bimodal and largely clustered around smaller sizes.

into a felsic magma chamber, causing viscous fingering of the new magma into the host magma, followed by brittle fragmentation of the fingers due to quenching. Likewise, Paredes-Mariño et al. (2017) analyzed the size distribution of enclave volumes to find $D_f$ of trachybasaltic fragments situated at the walls of vesicles (Fig. 6) of trachytic pumices from the Sete Cidades volcano (Azores) and found $D_f = 2.57$. Also, in agreement with Turcotte (1986), they proposed that the enclaves were formed by quenching and fracturing of the trachybasaltic magma, followed by increased heterogeneous bubble nucleation as the fragments acted as favorable nucleation sites, effectively enhancing eruption explosivity.

Hodge and Jellinek (2012) provided further evidence of the link between enclave formation and the rheology of the magma by analyzing enclaves from six lava domes and calculating the fractal dimension of fragmentation for each. They found that $D_f \sim 2$ and that there is a weak correlation between the fractal dimension and the viscosity contrasts of the mixing magmas, in that larger viscosity contrasts contribute to a higher fragmentation efficiency. Using the fractal dimensions, the median effective diameter of the enclave assemblies ($d_m$), and rheological and volcanological parameters, they concluded that the enclaves were formed in the tension regime, and they were able to divide their enclave populations in two groups: High-S and Low-S (named after the S-parameter, see Hodge and Jellinek, 2012), with High-S related to low $D_f$ and high $d_m$, and Low-S related to high $D_f$ and low $d_m$. In practice, the Low-S group would indicate a greater viscosity contrast between the mixing magmas, and a greater fragmentation efficiency, than the High-S group. The connection between fractal dimension and fragmentation efficiency is also corroborated by the work of Perugini and Kueppers (2012), who found that $D_f$ of pyroclasts increased with potential energy of fragmentation and with decreasing open porosity.

Finally, Glazner and Mills (2012) investigated the fractal dimension of fragmentation of mafic enclaves in the Half Dome granodiorite (Yosemite National Park) and found $D_f = 2.1$. They also note that while magma mixing seems to be a fractal process, this is only valid over a limited size range; further, if enclaves are formed by mafic magma being disassembled into drops in the felsic magma, the range of size distribution is dependent on the mafic dike aperture as well as subsequent recrystallization (Glazner and Mills, 2012, and references therein).

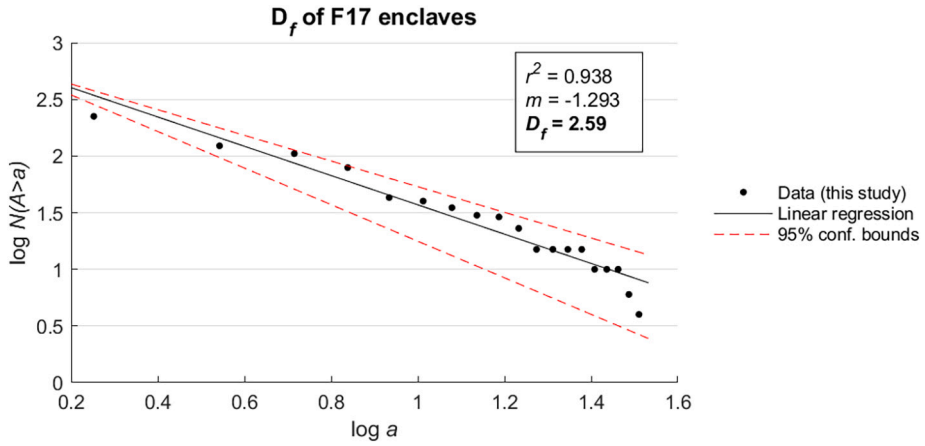


**Fig. 4.** The fractal analysis of the F17 enclaves using the data that is consistent with a linear relationship, as is shown in Fig. 2. The number of enclaves $N$ with an area $A$ larger than a comparative area $a$ is plotted against the comparative area. $D_f = -2m$ where $m$ is the slope of the line. The analysis yielded a linear relationship and $D_f = 2.59$. Dashed lines indicate upper (m = −1.638) and lower (m = −1.137) bound for 95% confidence (calculated using bootstrap resampling), corresponding to $D_f = 3.28$ and $D_f = 2.27$, respectively.

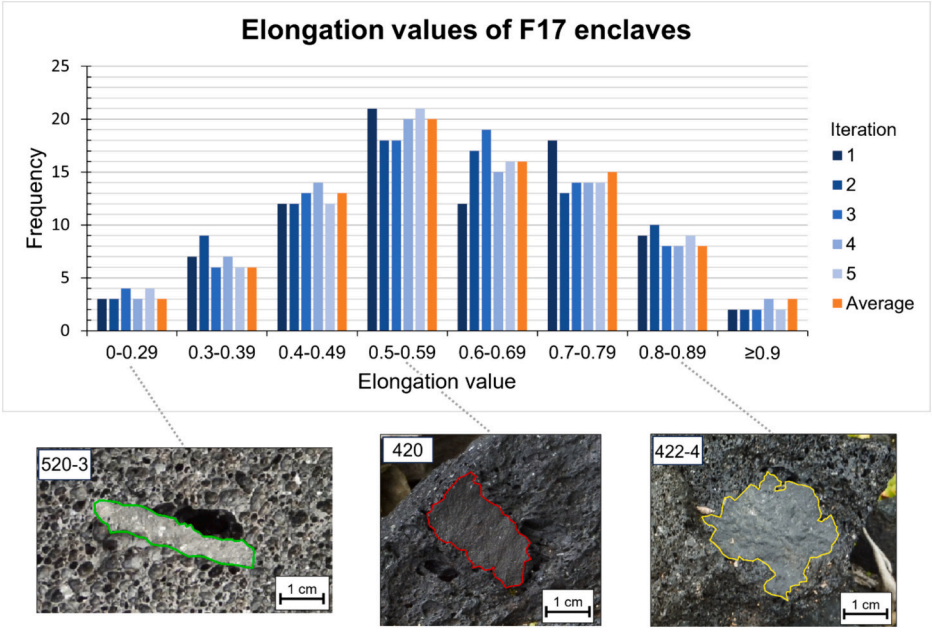


**Fig. 5.** Frequency histogram of elongation values for enclaves in all iterations, including the average of these iterations. Included are example pictures of enclaves with elongation values in the respective ranges.

The fractal dimension value $D_f = 2.59$ for the F17 enclaves analyzed in this study is consistent with previous studies of enclaves in lava (Fig. 6) as well as the work of Turcotte (1989). While this is only true for enclaves larger than 1 cm$^2$, the non-fractal size distribution of enclaves <1 cm$^2$ is likely the result of undersampling of small enclave sizes, a trend previously observed by Glazner and Mills (2012). Analyzing each iteration separately, the fractal dimension is somewhat lower ($D_f$ = 2.35–2.41). This is likely a direct result of using fewer data points, resulting in a larger number of large enclaves (which are already few in number) being excluded as $logN(A > a) = 0$. Indeed, when including enclaves for which $logN(A > a) = 0$, the values of $D_f$ are more consistent with that generated when analyzing all iterations together. The lower values are, however, more consistent with those of Hodge and Jellinek (2012).

The similarity between the result of this study and that of Turcotte (1989) may suggest that, similar to the samples of Fujiwara et al. (1977), the F17 enclaves were formed by brittle fragmentation, as has also been found by previous studies (Perugini et al., 2007; Paredes-Mariño et al., 2017), and thus exhibited solid-state behavior at the time of formation. From this assumption it follows that these enclaves do not necessarily represent areas of insufficient mixing (e.g. Perugini and Poli, 2000).

Perugini et al. (2007) deduced that the enclaves in their study were formed by disturbance of viscous fingers and compared this to the field evidence from Perugini and Poli (2005). Considering that the $D_f$ we found for F17 enclaves is similar to that found by Perugini et al. (2007) for Vulcano Island and Vegetation Island, it is reasonable to infer a similar mode of formation; however, there are three key differences between the F17 enclaves and those analyzed in previous studies (e.g. Perugini et al., 2007; Paredes-Mariño et al., 2017): (1) the glass compositions of the enclaves and the host magma are very similar (Soldati, pers. comm.), as opposed to previous studies which dealt with considerably larger ranges of silica content, and (2) microscopic images reveal that these enclaves do not display viscous textures to any large extent, but rather that they are very crystalline with plagioclase crystals at

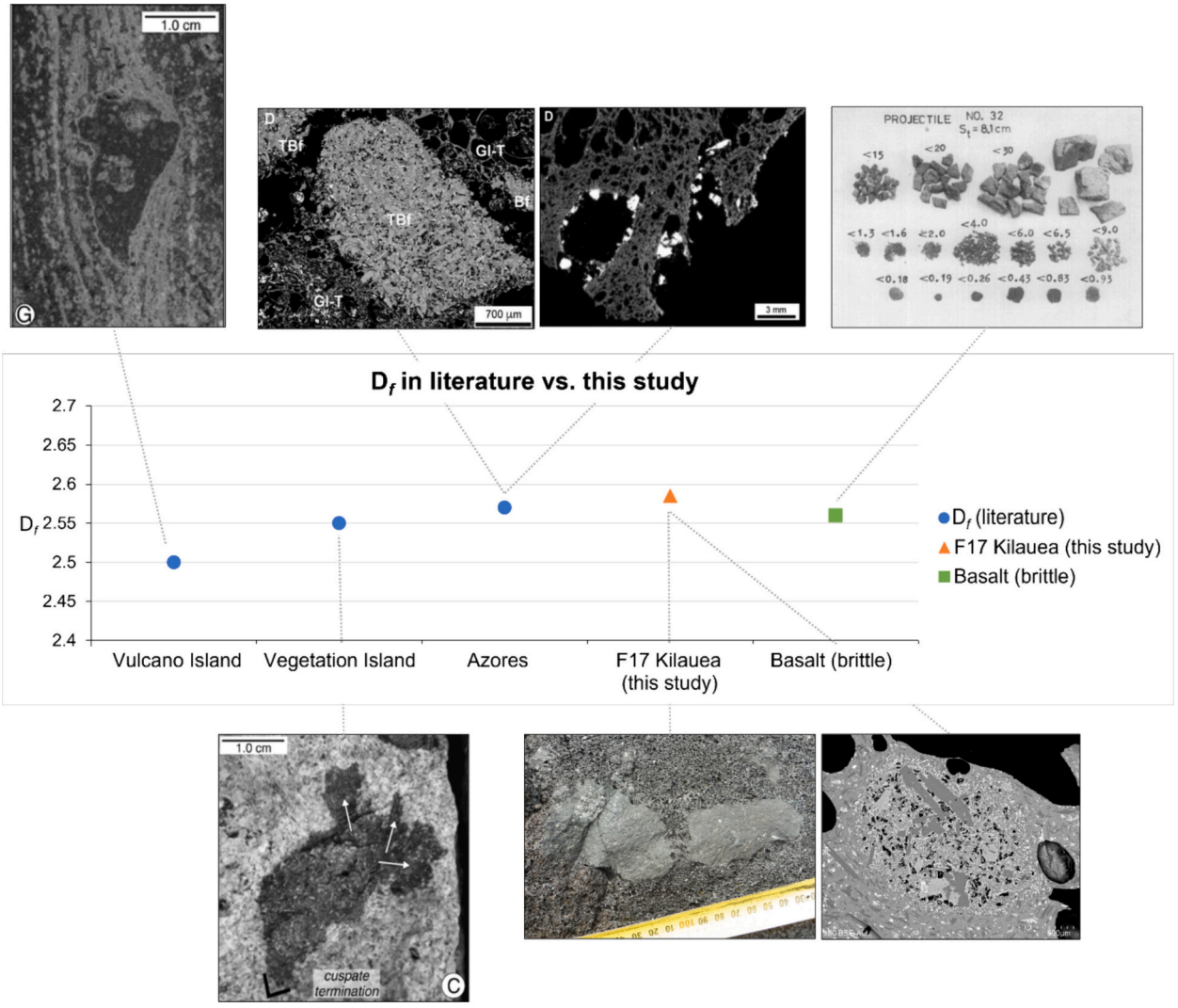


**Fig. 6.** Comparison of fractal analyses of enclaves and fragmented products in previous studies. The data show good agreement with the result in this study. Vulcano Island and Vegetation Island: Perugini et al. (2007). Azores: Paredes-Mariño et al. (2017). Basalt: Turcotte (1986).

places radiating outwards from the enclave, and that they lack signs of quenching (Soldati, pers. comm.). As such, the models presented in previous research may not be applicable to the case of F17. If the F17 enclaves were the result of magma mixing following the injection of magma into a pre-existing magma chamber, it is likely that the host magma would be more evolved in relation to the enclave magma than we see in the F17 samples. Since this is not the case, we infer that the enclaves most likely originated from a local mixing event where the LERZ magma under F17 was partially injected into an older pocket of magma, consistent with the findings of Soldati (pers. comm.). Furthermore, while viscous fingering and subsequent quenching of those fingers have been inferred by previous studies to be an important factor in the formation of enclaves, the highly crystalline nature of the F17 samples and the lack of viscous textures does not align with a large impact of viscous fingering. If the enclave magma was a mush with high crystallinity and high viscosity (Soldati, pers. comm.), this further points to a limited incidence of viscous fingering due to purely physical constraints. Additionally, the large range of elongation values found for the enclaves indicates the lack of any process acting uniformly to cause elongation. However, it should be noted that the F17 enclaves display generally lower elongation values, indicating a larger degree of elongation, compared to those of Perugini et al. (2007), adding further complexity to the role of viscous fingering.

Due to the above factors, a new model has to be considered to explain the formation of the enclaves in F17. This model must incorporate brittle fragmentation in the absence of quenching. Following the work of Hodge and Jellinek (2012), the median diameter of the F17 enclaves is consistent with the LS group, indicating efficient fragmentation and a high viscosity contrast, the latter which was noted by Soldati (pers. comm.) to be the reason why the enclaves and the host magma stayed distinct from each other. In the absence of viscous fingering, it is possible that the enclaves were formed by a process similar to magmatic stoping, which originally refers to incorporation of wall-rock into a magma chamber (Daly, 1933). It has previously been thought that stoping may play a role in magma hybridization as assimilation of wall-rock in the magma can have a large enough impact on the composition of the intruding magma to be observed in the erupted products (Furlong and Myers, 1985). This has, however, mainly been recognized to be a result of thermal stresses due to large temperature contrasts between the intruding magma and the wall-rock. While it is noteworthy that Soldati (pers. comm.) found evidence of hybridization-induced cooling of the host magma, possibly indicating a thermal contrast between the enclave and host magma in the F17 samples, MgO-geothermometry indicates similar temperatures for the two magmas, disproving that thermal stresses would have played a large role in the formation of the enclaves. Additionally, given that the calculated temperatures for the enclaves are

still well above the glass transition for andesitic magmas (Neuville et al., 1993) and the enclaves lack signs of quenching, it is not reasonable to assume that the solid behavior of the enclave magma originated from crossing of the glass transition due to a large temperature contrast during mixing, as would be the case for a mafic magma injected into a more evolved magma chamber.

Following the work of Dingwell (1996), the two most important factors that determine the rheological response of magma are the temperature and the timescale (strain rate). A higher temperature and a faster timescale promote fragmentation, while a lower temperature and a slower timescale promote quenching. Given the high temperatures calculated for the magmas, high strain rates, possibly caused by magma flow dynamics as the F17 magma was rising to the surface, must be invoked to explain the solid behavior and brittle fragmentation of the enclave magma. The high viscosity of the enclave magma would be more sensitive to fragmenting at high strain than a magma with lower viscosity would be due to a longer relaxation time (Dingwell and Webb, 1989). Therefore, we hypothesize that the hybridization occurred in a high-strain rate environment, enough for the enclave magma to transition into solid-state behavior and fragment in a brittle way (Fig. 7). Brittle fragmentation caused by locally high strain rates have been previously inferred by Gonnermann and Manga (2005) for fragments in obsidian from Big Glass Mountain (United States) and Mayor Island (New Zealand). Additionally, the solid behavior of the F17 enclaves may have been facilitated by the high crystallinity of the enclave magma, in agreement with the work of Namiki and Tanaka (2017) who found that a particle fraction over 0.4 yielded solid-like behavior of basaltic melts. After break-off, the enclaves would subsequently have been picked up by the F17 host magma and carried to the free surface.

This hypothesis agrees well with: (1) the unusually similar glass compositions of the two magmas, as the solid-state behavior can be explained by a high-strain rate environment imposed on a high-viscosity magma sensitive to high strain rates, and (2) the lack of quenching and viscous textures of the enclaves, indicating that they likely entered solid-state relatively quickly due to high strain-rates, as opposed to a rapid temperature decrease causing quenching. Further modification of the enclaves after break-off, such as described by Paredes-Mariño et al. (2017) by the nucleation of bubbles on the fragments, or increased elongation, are not inferred from the F17 samples.

The enclaves in F17 represent a unique process in which enclaves were formed not by injection of a mafic magma into an evolved magma chamber, but by local hybridization of two compositionally similar magmas. This suggests that magmatic enclaves may form across a wide range of magmatic end members, including ones very similar to each other. Additionally, the solid-state behavior of the enclaves despite high temperatures once again emphasizes the importance of considering strain rates in volcanic systems.

## 5. Conclusions

Fractal analysis of the size distribution of enclaves in the F17 lava indicates that they were formed by brittle fragmentation. The small compositional difference between the host and the enclave magma, and the lack of quenching and viscous textures of the enclaves, sets these enclaves apart from those of previous studies and requires a new model to explain the enclave formation. Given that the temperatures inferred from previous studies are inconsistent with the enclave magma approaching the glass transition, high strain rates must be invoked to explain the brittle fragmentation. We hypothesize that the strain rates during the magma hybridization were high enough to cause the enclave magma to transition into solid-state behavior, facilitated by its high viscosity and crystallinity. This allowed for brittle fragmentation of the enclave magma, causing fragments to break off and be picked up by the F17 host magma.

The result of this study indicates a unique process by which the F17 enclaves were formed by brittle fragmentation due to high strain rates during magma hybridization between two compositionally similar magmas, as opposed to quenching caused by injection of primitive magma into an evolved magma chamber. Additionally, this study highlights the impact of strain rates on magma rheology.

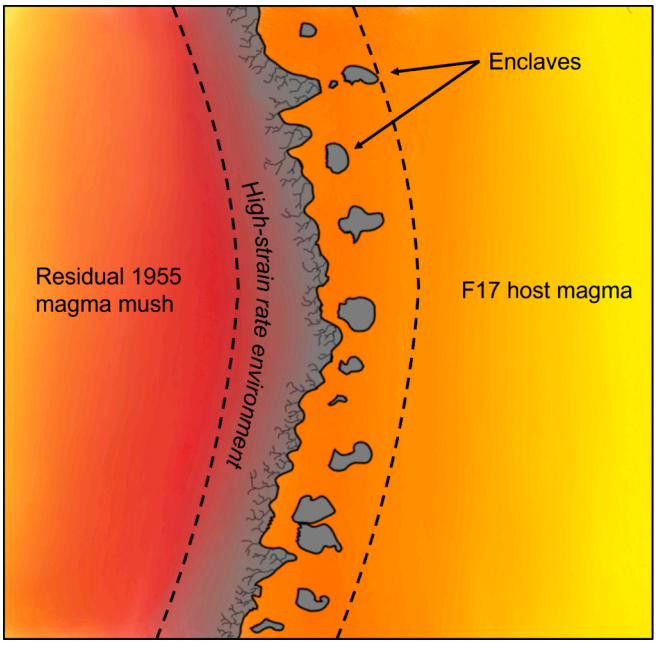


**Fig. 7.** Schematic illustration of the formation of the F17 enclaves. The hybridization between the F17 host magma and the residual magma mush pocket occurred in a high-strain rate environment, causing brittle fragmentation of the magma mush and the break-off of enclaves.

## CRediT authorship contribution statement

**V. Haag:** Writing – original draft, Visualization, Validation, Methodology, Investigation, Formal analysis, Data curation. **B.F. Houghton:** Writing – review & editing, Resources, Funding acquisition. **D. Perugini:** Writing – review & editing, Methodology, Conceptualization. **A. Soldati:** Writing – review & editing, Validation, Supervision, Resources, Project administration, Funding acquisition, Conceptualization.

## Declaration of competing interest

The authors declare that they have no known competing financial interests or personal relationships that could have appeared to influence the work reported in this paper.

## Data availability

Data will be made available on request.

## Acknowledgements

V.H., B.H., and A.S. wish to acknowledge the support of NSF grant EAR-2119973.

## Appendix A. Supplementary data

Supplementary data to this article can be found online at https://doi.org/10.1016/j.jvolgeores.2024.108087.

## References

Bennet, J.G., 1936. Broken coal. J. Inst. Fuel 10, 23–39.

Bruno, B.C., Taylor, G.J., Rowland, S.K., Lucey, P.G., Self, S., 1992. Lava flows are fractals. Geophys. Res. Lett. 19 (3), 305–308.
Daly, R.A., 1933. Igneous Rocks and the Depths of the Earth. McGraw-Hill, New York, p. 598.
Dingwell, D.B., 1996. Volcanic dilemma–flow or blow? Science 273 (5278), 1054–1055.
Dingwell, D.B., Webb, S.L., 1989. Structural relaxation in silicate melts and non-Newtonian melt rheology in geologic processes. Phys. Chem. Miner. 16, 508–516.
Fujiwara, A., Kamimoto, G., Tsukamoto, A., 1977. Destruction of basaltic bodies by high-velocity impact. Icarus 31 (2), 277–288.
Furlong, K.P., Myers, J.D., 1985. Thermal-mechanical modeling of the role of thermal stresses and stoping in magma contamination. J. Volcanol. Geotherm. Res. 24 (1–2), 179–191.
Gansecki, C., Lee, R.L., Shea, T., Lundblad, S.P., Hon, K., Parcheta, C., 2019. The tangled tale of Kīlauea's 2018 eruption as told by geochemical monitoring. Science 366 (6470), eaaz0147.
Glazner, A.F., Mills, R.D., 2012. Interpreting two-dimensional cuts through broken geologic objects: fractal and non-fractal size distributions. Geosphere 8 (4), 902–914.
Gonnermann, H.M., Manga, M., 2005. Flow banding in obsidian: a record of evolving textural heterogeneity during magma deformation. Earth Planet. Sci. Lett. 236 (1–2), 135–147.
Helz, R.T., Thornber, C.R., 1987. Geothermometry of Kilauea Iki lava lake, Hawaii. Bull. Volcanol. 49, 651–668.
Ho, R.A., Garcia, M.O., 1988. Origin of differentiated lavas at Kilauea Volcano, Hawaii: Implications from the 1955 eruption. Bull. Volcanol. 50, 35–46.
Hodge, K.F., Jellinek, A.M., 2012. Linking enclave formation to magma rheology. J. Geophys. Res. Solid Earth 117 (B10).
Katz, A., Thompson, A.H., 1985. Fractal sandstone pores: implications for conductivity and pore formation. Phys. Rev. Lett. 54 (12), 1325.
Mandelbrot, B.B., 1982. The Fractal Geometry of Nature. W.H. Freeman, New York, p. 468.
Manning, C.E., 1994. Fractal clustering of metamorphic veins. Geology 22 (4), 335–338.
Namiki, A., Tanaka, Y., 2017. Oscillatory rheology measurements of particle-and bubble-bearing fluids: Solid-like behavior of a crystal-rich basaltic magma. Geophys. Res. Lett. 44 (17), 8804–8813.
Neal, C.A., Brantley, S.R., Antolik, L., Babb, J.L., Burgess, M., Calles, K., Cappos, M., Chang, J.C., Conway, S., Desmither, L., Dotray, P., Elias, T., Fukunaga, P., Fuke, S., Johanson, I.A., Kamibayashi, K., Kauahikaua, J., Lee, R.L., Pekalib, S., Miklius, A., Million, W., Moniz, C.J., Nadeau, P.A., Okubo, P., Parcheta, C., Patrick, M.P., Shiro, B., Swanson, D.A., Tollett, W., Trusdell, F., Younger, E.F., Zoeller, M.H., Montgomery-Brown, E.K., Anderson, K.R., Poland, M.P., Ball, J., Bard, J., Coombs, M., Dietterich, H.R., Kern, C., Thelen, W.A., Cervelli, P.F., Orr, T., Houghton, B.F., Gansecki, C., Hazlett, R., Lundgren, P., Diefenbach, A.K., Lerner, A. H., Waite, G., Kelly, P., Clor, L., Werner, C., Mulliken, K., Fisher, G., 2018. The 2018 rift eruption and summit collapse of Kīlauea Volcano. Science 363 (6425), 367–374.
Neuville, D.R., Courtial, P., Dingwell, D.B., Richet, P., 1993. Thermodynamic and rheological properties of rhyolite and andesite melts. Contrib. Mineral. Petrol. 113, 572–581.
Paredes-Mariño, J., Dobson, K.J., Ortenzi, G., Kueppers, U., Morgavi, D., Petrelli, M., Hess, K.-U., Laeger, K., Porreca, M., Pimentel, A., Perugini, D., 2017. Enhancement of eruption explosivity by heterogeneous bubble nucleation triggered by magma mingling. Sci. Rep. 7 (1), 16897.
Patrick, M.R., Dietterich, H.R., Lyons, J.J., Diefenbach, A.K., Parcheta, C., Anderson, K. R., Namiki, A., Sumita, I., Shiro, B., Kauahikaua, J.P., 2019. Cyclic lava effusion during the 2018 eruption of Kīlauea Volcano. Science 366 (6470), eaay9070.
Perugini, D., Kueppers, U., 2012. Fractal analysis of experimentally generated pyroclasts: a tool for volcanic hazard assessment. Acta Geophys. 60, 682–698.
Perugini, D., Poli, G., 2000. Chaotic dynamics and fractals in magmatic interaction processes: a different approach to the interpretation of mafic microgranular enclaves. Earth Planet. Sci. Lett. 175 (1–2), 93–103.
Perugini, D., Poli, G., 2005. Viscous fingering during replenishment of felsic magma chambers by continuous inputs of mafic magmas: field evidence and fluid-mechanics experiments. Geology 33 (1), 5–8.
Perugini, D., Valentini, L., Poli, G., 2007. Insights into magma chamber processes from the analysis of size distribution of enclaves in lava flows: a case study from Vulcano Island (Southern Italy). J. Volcanol. Geotherm. Res. 166 (3–4), 193–203.
Pietruszka, A.J., Garcia, M.O., Rhodes, J.M., 2021. Accumulated Puʻu ʻŌʻō magma fed the voluminous 2018 rift eruption of Kīlauea Volcano: evidence from lava chemistry. Bull. Volcanol. 83, 1–18.
Roduit, N. JMicroVision: Image analysis toolbox for measuring and quantifying components of high-definition images. Version 1.3.4. https://jmicrovision.github.io (accessed July 2022).
Schoutens, J.E., 1979. Empirical analysis of nuclear and high-explosive cratering and ejecta. In: Nuclear Geoplosics Sourcebook, 55, part 2, section 4, Rep. DNA 65 01H-4-2, Del. Nucl. Agency, Bethesda, Md.
Soldati, A., Houghton, B.F., Dingwell, D.B., 2021. A lower bound on the rheological evolution of magmatic liquids during the 2018 Kilauea eruption. Chem. Geol. 576, 120272.
Sreenivasan, K.R., Prasad, R.R., 1989. The fractal dimension of scalar surfaces in turbulent jets. Fluid Dynam. Trans. 14, 205–218.
Turcotte, D.L., 1986. Fractals and fragmentation. J. Geophys. Res. Solid Earth 91 (B2), 1921–1926.
Turcotte, D.L., 1989. Fractals in geology and geophysics. Pure Appl. Geophys. 131, 171–196.
Walker, B.H., Houghton, B.F., Llewellin, E.W., 2023. Coexisting Strombolian and Hawaiian activity during the 2018 fissure eruption of Kīlauea–Implications for processes of weak explosions. J. Volcanol. Geotherm. Res. 435, 107754.
Wright, T.L., Fiske, R.S., 1971. Origin of the differentiated and hybrid lavas of Kilauea volcano, Hawaii. J. Petrol. 12 (1), 1–65.